Engineering 5 (2019) 730–735

Contents lists available at ScienceDirect

Engineering

journal homepage: www.elsevier.com/locate/eng

Research
Additive Manufacturing—Article

Data-Driven Microstructure and Microhardness Design in Additive Manufacturing Using a Self-Organizing Map

Zhengtao Gan [a,*], Hengyang Li [a], Sarah J. Wolff [a], Jennifer L. Bennett [a,b], Gregory Hyatt [b], Gregory J. Wagner [a], Jian Cao [a], Wing Kam Liu [a,*]

[a] Department of Mechanical Engineering, Northwestern University, Evanston, IL 60208, USA
[b] DMG MORI, Hoffman Estates, IL 60192, USA

ARTICLE INFO

Article history:
Received 13 August 2018
Revised 9 December 2018
Accepted 1 March 2019
Available online 2 July 2019

Keywords:
Additive manufacturing
Data science
Multiphysics modeling
Self-organizing map
Microstructure
Microhardness
Ni-based superalloy

ABSTRACT

To design microstructure and microhardness in the additive manufacturing (AM) of nickel (Ni)-based superalloys, the present work develops a novel data-driven approach that combines physics-based models, experimental measurements, and a data-mining method. The simulation is based on a computational thermal-fluid dynamics (CtFD) model, which can obtain thermal behavior, solidification parameters such as cooling rate, and the dilution of solidified clad. Based on the computed thermal information, dendrite arm spacing and microhardness are estimated using well-tested mechanistic models. Experimental microstructure and microhardness are determined and compared with the simulated values for validation. To visualize process–structure–properties (PSPs) linkages, the simulation and experimental datasets are input to a data-mining model—a self-organizing map (SOM). The design windows of the process parameters under multiple objectives can be obtained from the visualized maps. The proposed approaches can be utilized in AM and other data-intensive processes. Data-driven linkages between process, structure, and properties have the potential to benefit online process monitoring control in order to derive an ideal microstructure and mechanical properties.

1. Introduction

Accelerating the process and materials design in additive manufacturing (AM) has been investigated in the current literature (e.g., Refs. [1–3]). In this respect, multiscale and multiphysics modeling and simulation are vital, because they have the potential to significantly reduce the cost and time expended in experiments [4,5]. Many efforts have been made to model and simulate AM processes in order to predict process–structure–property (PSP) relationships [6–9]. Meanwhile, it is critical for model validation and verification to employ highly controlled experimental measurements, which include online monitoring of the process, microstructure characterization, and mechanical testing [10–12].

However, merely combining experiments with simulations cannot achieve the desired acceleration in AM process and materials design, because it is difficult to understand and utilize the high-dimensional datasets produced by simulations and experiments. There is an essential need for supportive data science approaches that efficiently integrate the iterations between experiments and multiscale simulation. Popova et al. [13] used data science approaches to understand the process–structure linkages in AM, and used a proposed data science workflow in an attempt to understand the relationships between process conditions and synthetic grain structure. An integration of physics-based and data-mining approaches for temperature field prediction in AM has been proposed [14,15]. A surrogate model based on a functional Gaussian process was calibrated by means of three-dimensional (3D) finite-element analysis (FEA) and experimental thermal image data [14,15]. Salloum et al. [16] undertook high-dimensional dataset compression by using adaptive Alpert tree wavelets in the laser-engineered net shape (LENS) process. The self-organizing map (SOM), which was proposed by Kohonen [17,18], is an unsupervised machine learning algorithm based on neural networks that is able to map high-dimensional data to two-dimensional (2D) planes while preserving topology [19,20]. Compared with an artificial neural network

* Corresponding authors.
E-mail addresses: zhengtao.gan@northwestern.edu (Z. Gan), w-liu@northwestern.edu (W.K. Liu).

https://doi.org/10.1016/j.eng.2019.03.014

(ANN), which is commonly used for regression problems, the main advantage of the SOM is that it can visualize high-dimensional data in the form of a low-dimensional map, which helps researchers to visually identify underlying relations between the features. As a tool to visualize high-dimensional datasets, the SOM is beneficial for the cluster analysis of real-life design problems as well [21].

In this study, an SOM is used to visualize high-dimensional data in AM; these data are obtained from well-designed experimental measurements and multiphysics models. The SOM is introduced to find the relationships among laser power, mass flow rate, energy density, dilution, cooling rate, dendrite arm spacing, and microhardness in AM. In addition, the design windows of process parameters under multiple objectives can be obtained from the visualized SOM. A schematic diagram of this work is shown in Fig. 1 [22].

2. Experimental dataset

Single tracks of Inconel 718 powder were deposited on an AISI 1045 carbon steel disc using a 1020 nm high-powered continuous wave laser. The beam diameter at its focus is 3 mm. The laser power was set to be constant, while the mass flow rate was incremented from 3.35 to 27.2 g·min^{-1} in 2.65 g·min^{-1} increments. At each mass flow rate, the laser power was incremented from 1000 to 2000 W in 200 W increments, resulting in 60 single tracks. The detailed process parameters and conditions can be found in our previous paper [10]. Materials characterization in this case included CR measurements, dilution measurements, dendrite arm spacing measurements, and hardness testing. An infrared thermal camera was used to determine the cooling rate from the solidus to liquidus temperature of the steady-state melt pool, as detailed in Ref. [10]. After etching the clad cross-section, dilution and dendrite arm spacing can be identified and quantified. Vickers microhardness measurements were taken to obtain the averaged microhardness. A summary of the experimental efforts as well as a chart detailing the dilution are provided in Fig. 2. Details of experiments can be found in Ref. [22].

3. Physics-based simulation dataset

A computational thermal-fluid dynamics (CtFD) model was developed to simulate the directed energy deposition (DED) process [23]. The current paper does not describe the modeling equations, but rather provides a few features to offer an understanding of the CtFD model and process–structure models. The non-isothermal Navier–Stokes (N–S) equations, which include mass, momentum, and energy equations, were solved to obtain the temperature field and liquid metal flow in the melt pool [24,25]. A physics-based arbitrary Lagrangian–Eulerian (ALE) method was utilized to track the free surface of the melt pool [23]. The melt pool dimensions, dilution, and cooling rate at the liquid–solid interface can be computed based on the steady-state melt pool temperature field. Dendrite arm spacing is evaluated by the Hurt formula [26]. Vickers hardness (HV) can be determined by the

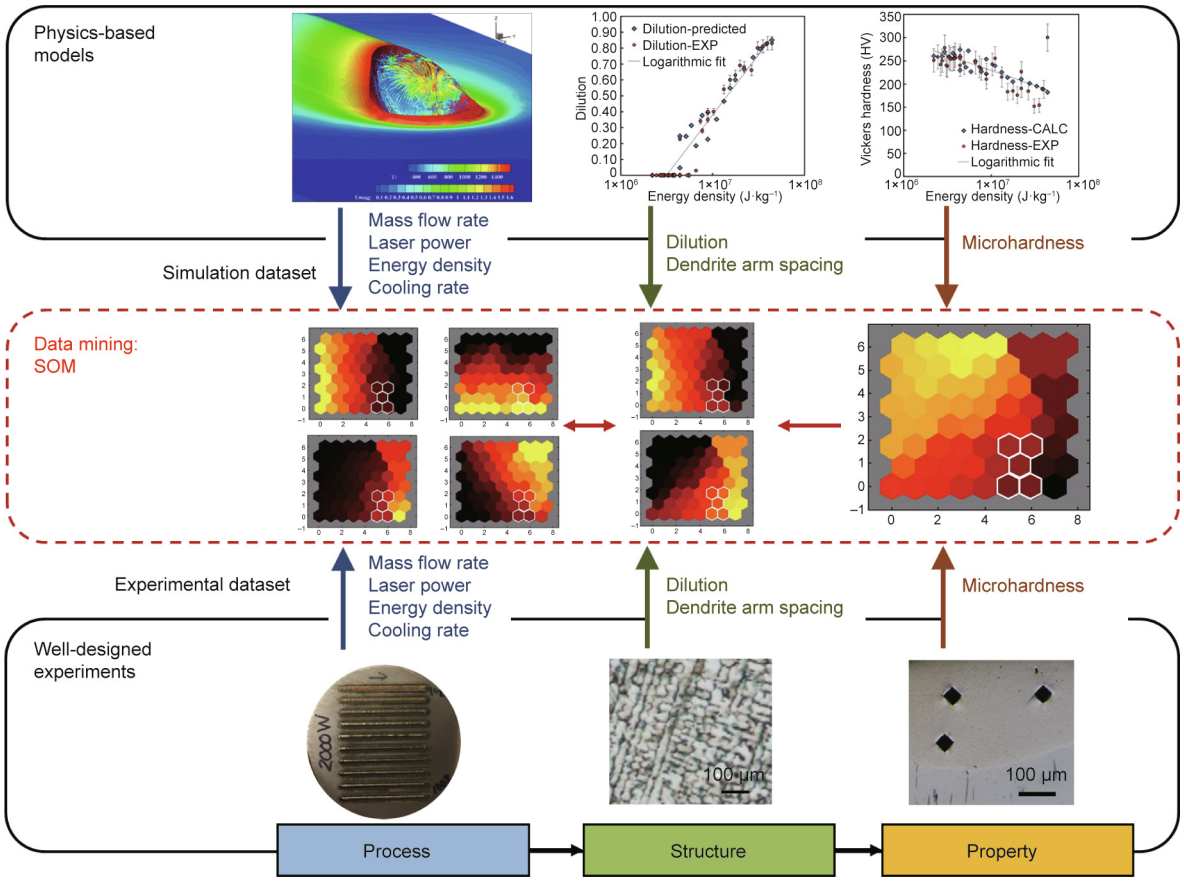

Fig. 1. A schematic description of the workflow typically employed in current computational efforts (top row) and of experimental efforts (bottom row), along with a description of how this can be augmented with a data-mining approach to recover high-value PSP linkages of interest to material innovation efforts. CALC: calculated; EXP: experiment.

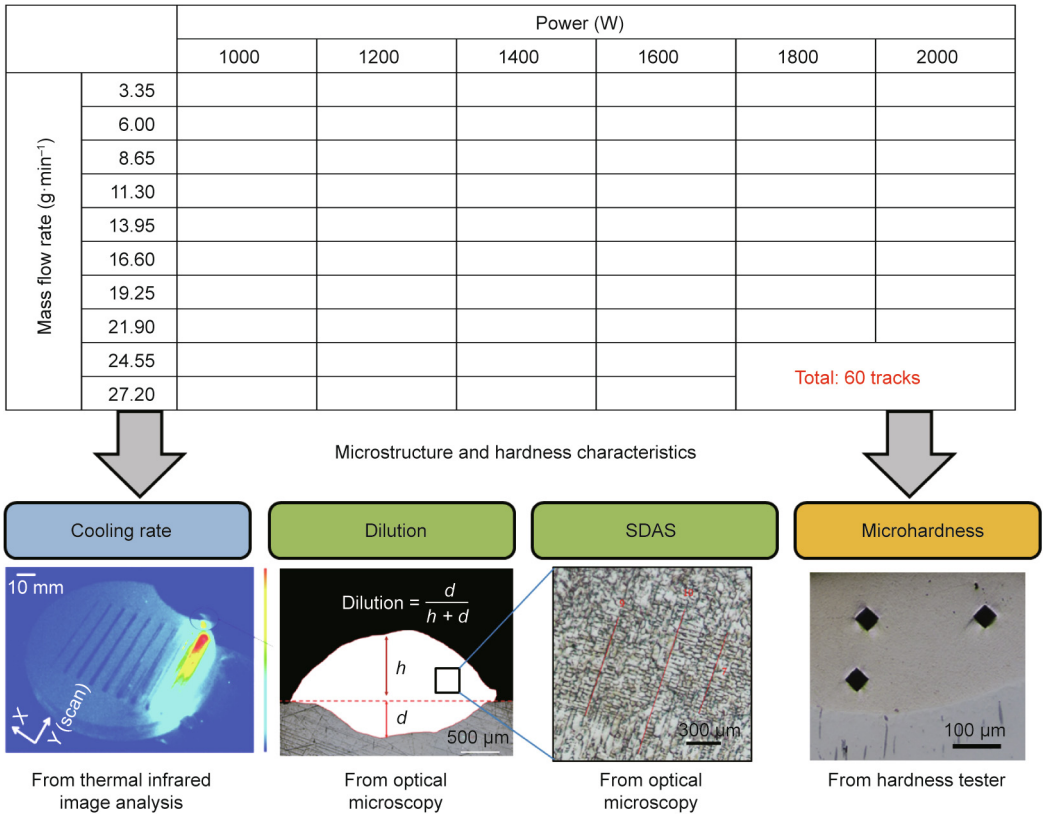

Fig. 2. Orthogonal views of the experimental dataset with variable laser power and mass flow rate, and four resulting measurement outputs: cooling rate, dilution, secondary dendrite arm spacing (SDAS), and microhardness, from microstructure and hardness characterization.

nickel (Ni) equivalent for Ni-based superalloys [27]. Details of these models have been described in our previous work [22]. In total, 25 simulation cases with various laser power levels and mass flow rates were computed. For each case, the structures and properties observed were the melt pool geometry, dilution, cooling rate, secondary dendrite arm spacing (SDAS), and microhardness. A summary of the simulation efforts is shown in Fig. 3.

4. Data mining for visualizing PSPs linkages

The SOM Toolbox in MATLAB [28] was used to simultaneously visualize high-dimensional datasets and design process parameters. Using physics-based simulations and experimental measurements, seven-dimensional (7D) PSP datasets were obtained for data mining as the input vector, $\boldsymbol{x}_m$, as shown in

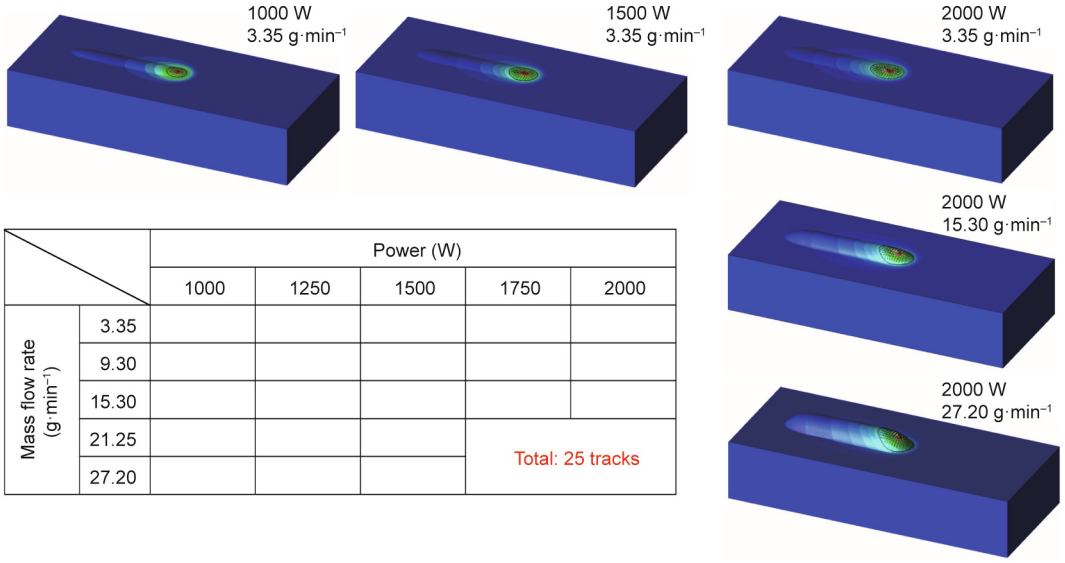

Fig. 3. Orthogonal views of the simulation dataset with variable laser power and mass flow rate, along with selected simulation results.

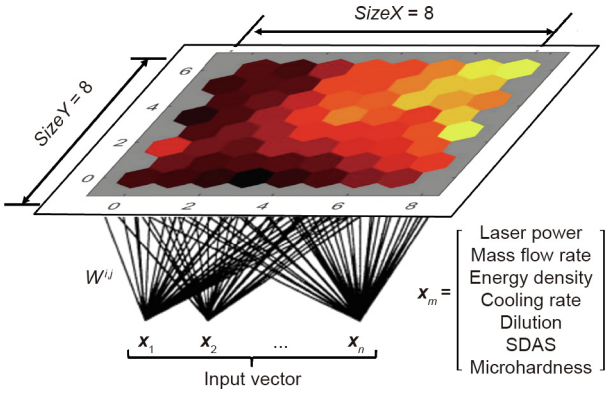

Fig. 4. A typical SOM including input vectors. n: total datasets; $W^{i,j}$: weight.

Fig. 4. Because the simulation results agree well with the experimental results [22], 25 simulation data points and five experimental data points were used as input vectors to train a single 8×8 SOM indistinctively. We compared the results from differently sized SOMs, and found that the 8×8 SOM has the best performance. If the map size is too small, the map resolution is very low; however, an SOM that is too large results in overfitting. Each 7D input vector contains seven variables, including: four process variables (i.e., laser power, mass flow rate, energy density, and cooling rate), two microstructure variables (i.e., dilution and SDAS), and one property variable (i.e., microhardness). In this illustrative case, only five experimental data points were used as the input of the SOM out of the total 60 experimental points, because only five experimental data points have all seven measurements. The current version of the SOM requires data points with the same dimension of features. Therefore, the rest of the experimental data are used to validate the simulation results, rather than train the SOM. The goal of this work is to demonstrate a data-driven workflow in order to understand and design high-dimensional datasets in AM. There is potential for more experimental and simulation datasets to be involved in order to obtain better map resolution without changing the workflow.

The training procedure can be described by the pseudo code, as shown in **Algorithm 1**. The map neurons are hexagonal. The labels of the X and Y axes are the integers $1 \le i \le SizeX$, and $1 \le j \le SizeY$, respectively, as shown in Fig. 4. Initially, the weights of the neurons are set to be $W_0^{i,j}$ with random number [0, 1]. The elements of each input vector are normalized linearly to [0, 1]. After initialization, the SOM is trained for a number of T epochs. For the current epoch t and each input vector $\boldsymbol{x}_m$, first, the best matching unit (BMU) is determined by calculating the distance between the input vector and each neuron weight using Eq. (1). The BMU is a map unit has the shortest distance to input vector $\boldsymbol{x}_m$. Second, the diameter of the neighborhood around the BMU can be determined by Eq. (2), where $d(t)$ is a function that decreases monotonously with time. The initial distance coefficient is d_0 and is 8 in this study. The decrease rate is λ. Third, the weights $W_m^{i,j}$ in the BMU and its neighborhoods are updated according to Eqs. (3) and (4). In Eqs. (3) and (4), $h_{\mathrm{BMU},i,j}$ represents the Gaussian kernel function, where $\alpha(t)$ is a learning rate parameter, $r_{i,j}$ is the position of each unit, and r_{BMU} is the position of the BMU. The current epoch is finished after all the $\boldsymbol{x}_m$ have been calculated to the SOM. By selecting a large enough number of epochs $T = 100$ in this case, the SOM can converge. Fig. 5 presents the variance of weights of the neuron points as a function of the epoch, indicating the convergence of the trained SOM. When training is finished, the map can reorder the original datasets while preserving the topological properties of the input space.

Algorithm 1. Program SOM

Initialize weights of neurons $W_0^{i,j}$ with random number [0, 1]
Index of epoch: t
Index of input vector in the dataset: m
Do $t = 0$ to T (max index of epoch)
  Do $m = 1$ to n (max index of input vector)
    Find BMU:

$$W_m^{\mathrm{BMU}} = \underset{\substack{i=1\ldots SizeX \\ j=1\ldots SizeY}}{\arg\min} \parallel W_m^{i,j} - \boldsymbol{x}_m \parallel^2 \quad (1)$$

    Determine diameter of neighborhood around BMU:

$$d(t) = d_0 \exp(-t/\lambda) \quad (2)$$

    Update weights $W_{m+1}^{i,j}$ in BMU and neighborhoods:

$$W_{m+1}^{i,j} = W_m^{i,j} + h_{\mathrm{BMU},i,j}\left(\boldsymbol{x}_m - W_m^{i,j}\right) \quad (3)$$

$$h_{\mathrm{BMU},i,j} = \alpha(t)\exp\left\{-\parallel r_{i,j} - r_{\mathrm{BMU}} \parallel^2 / \left[2d^2(t)\right]\right\} \quad (4)$$

  End do
End do

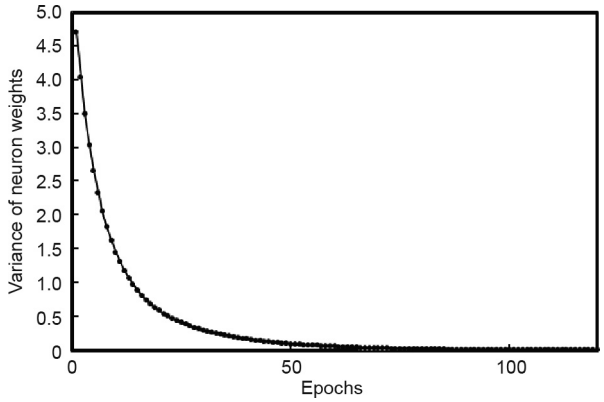

Fig. 5. Variance–epoch curve of the trained SOM.

Each map is shown in Fig. 6. The relation between the PSP variables can be understood visually. For example, as shown in Fig. 6, the mass flow rate and SDAS are positively correlated, as the component planes of the mass flow rate and SDAS have similar values at similar positions. Conversely, the mass flow rate and dilution are highly negatively correlated. Thus, according to the visualized SOM in Fig. 6, the following results are obtained in this study:

- The mass flow rate, more than laser power, greatly contributes to the cooling rate and SDAS.
- The dilution and microhardness depend on both the mass flow rate and laser power.
- The microhardness is dominated by the dilution, rather than by the SDAS or cooling rate.

Obtained through the data-mining approach, these elations provide valuable insight into the complex underlying physical phenomena and material evolution during the AM process. In addition, it is possible to obtain the desired process parameter window with multiple objective microstructure and property ranges. In this study, the objective dilution is from 0.1 to 0.3. In this range of dilution, the solidified track can avoid both lack of fusion due to low dilution and property degradation due to high dilution [29]. The SDAS should be minimized and the microhardness should be maximized in order to maintain good mechanical properties. An iteration procedure through all the units is undertaken in order to seek units that satisfy these restrictions. An objective cluster

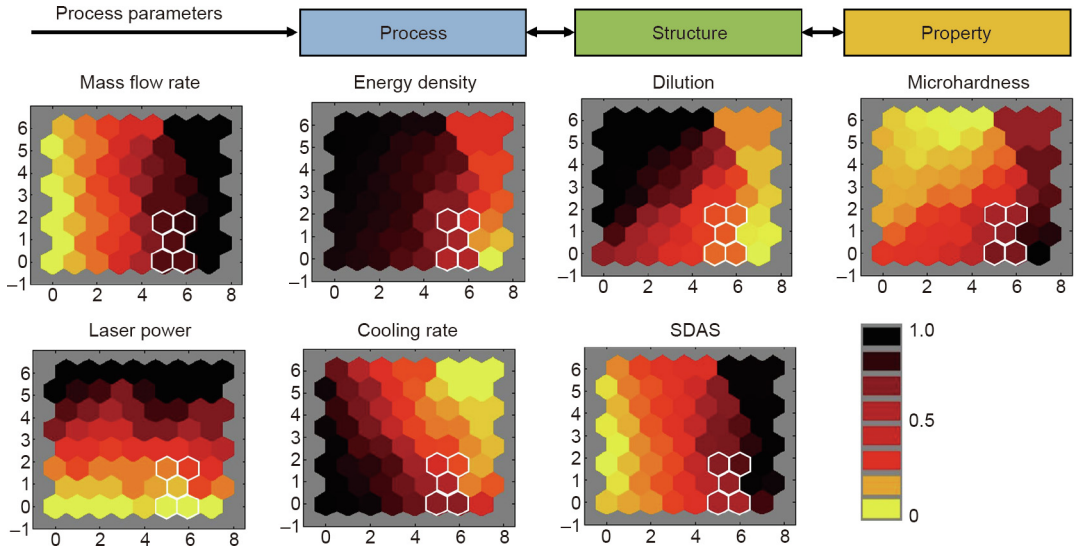

Fig. 6. Contour plots of all design variables with the optimized design window outlined by a white wireframe.

that includes multiple units can be selected as a white wireframe, as shown in Fig. 6. Thus, the following desired process parameters can be obtained: a laser power ranging from 1000 to 1100 W and a mass flow rate ranging from 22.4 to 24.8 $g \cdot min^{-1}$. The desired energy density, which is defined as laser power divided by mass flow rate, ranges from 2.4×10^6 to 2.9×10^6 $J \cdot kg^{-1}$.

The effect of uncertainties, such as the simulation error, on the fidelity of the SOM is an interesting and important topic. In our future work, a modified SOM with uncertain inputs will be investigated by using a larger database.

5. Conclusion

This work presented a novel workflow to produce, visualize, and design high-dimensional PSP linkages in AM through the utilization of multiphysics modeling, experimental measurements, and advanced data science techniques. An application of this workflow to quantify and design microstructure and microhardness was demonstrated herein. High-dimensional datasets, which include laser power, mass flow rate, energy density, cooling rate, dilution, dendrite arm spacing, and microhardness, were derived by means of physics-based models and experiments. The profound relations among PSP data were visualized using an SOM, and important relationship trends were identified. Multiple objective optimization examples were proposed and solved in order to attain desired process parameters. The presented approach can be applied to a broad variety of PSP datasets for AM and other data-intensive processes. Data-driven relationships between process, structure, and property can provide online monitoring and process control to derive ideal microstructure and mechanical properties.

Acknowledgements

Jian Cao, Gregory J. Wagner, and Wing K. Liu acknowledge support from the National Science Foundation (NSF) Cyber–Physical Systems (CPS) (CPS/CMMI-1646592). Hengyang Li acknowledges support from the Northwestern Data Science Initiative (DSI; 171474500210043324). Jian Cao, Gregory J. Wagner, Wing K. Liu, Jennifer L. Bennett, and Sarah J. Wolff acknowledge support from the Digital Manufacturing and Design Innovation Institute (DMDII;15-07). Jian Cao, Wing K. Liu, Zhengtao Gan, and Jennifer L. Bennett acknowledge support from the Center for Hierarchical Materials Design (CHiMaD; 70NANB14H012). This work made use of facilities at DMG MORI and Northwestern University. It also made use of the MatCI Facility, which receives support from the MRSEC Program (NSF DMR-168 1720139) of the Materials Research Center at Northwestern University.

Compliance with ethics guidelines

Zhengtao Gan, Hengyang Li, Sarah J. Wolff, Jennifer L. Bennett, Gregory Hyatt, Gregory J. Wagner, Jian Cao, and Wing Kam Liu declare that they have no conflict of interest or financial conflicts to disclose.

References

[1] Breneman CM, Brinson LC, Schadler LS, Natarajan B, Krein M, Wu K, et al. Stalking the materials genome: a data-driven approach to the virtual design of nanostructured polymers. Adv Funct Mater 2013;23(46):5746–52.
[2] McDowell DL, Kalidindi SR. The materials innovation ecosystem: a key enabler for the materials genome initiative. MRS Bull 2016;41(4):326–37.
[3] Jain A, Ong SP, Hautier G, Chen W, Richards WD, Dacek S, et al. Commentary: the materials project: a materials genome approach to accelerating materials innovation. APL Mater 2013;1(1):011002.
[4] Thompson SM, Bian L, Shamsaei N, Yadollahi A. An overview of direct laser deposition for additive manufacturing; part I: transport phenomena, modeling and diagnostics. Addit Manuf 2015;8:36–62.
[5] David SA, DebRoy T. Current issues and problems in welding science. Science 1992;257(5069):497–502.
[6] Smith J, Xiong W, Yan W, Lin S, Cheng P, Kafka OL, et al. Linking process, structure, property, and performance for metal-based additive manufacturing: computational approaches with experimental support. Comput Mech 2016;57(4):583–610.
[7] He X, Mazumder J. Transport phenomena during direct metal deposition. J Appl Phys 2007;101(5):053113.
[8] Gan Z, Yu G, He X, Li S. Numerical simulation of thermal behavior and multicomponent mass transfer in direct laser deposition of co-base alloy on steel. Int J Heat Mass Transfer 2017;104:28–38.
[9] Gan Z, Yu G, Li S, He X, Chen R, Zheng C, et al. A novel intelligent adaptive control of laser-based ground thermal test. Chin J Aeronaut 2016;29(4):1018–26.
[10] Gan Z, Lian Y, Lin SE, Jones KK, Liu WK, Wagner GJ. Benchmark study of thermal behavior, surface topography, and dendritic microstructure in selective laser melting of inconel 625. Integr Mater Manuf Innovation 2019;8(2):178–93.
[11] Wolff SJ, Lin S, Faierson EJ, Liu WK, Wagner GJ, Cao J. A framework to link localized cooling and properties of directed energy deposition (DED)-processed Ti–6Al–4V. Acta Mater 2017;132:106–17.

[12] Wolff S, Lee T, Faierson E, Ehmann K, Cao J. Anisotropic properties of directed energy deposition (DED)-processed Ti–6Al–4V. J Manuf Process 2016;24:397–405.
[13] Popova E, Rodgers TM, Gong X, Cecen A, Madison JD, Kalidindi SR. Process-structure linkages using a data science approach: application to simulated additive manufacturing data. Integr Mater Manuf Innov 2017;6(1):54–68.
[14] Li J, Jin R, Yu HZ. Integration of physically-based and data-driven approaches for thermal field prediction in additive manufacturing. Mater Des 2018;139:473–85.
[15] Hu Z, Wang H, Thouless MD, Lu W. An approach of adaptive effective cycles to couple fretting wear and creep in finite-element modeling. Int J Solids Struct 2018;139–140:302–11.
[16] Salloum M, Johnson KL, Bishop JE, Aytac JM, Dagel D, Van Bloemen Waanders BG. Adaptive wavelet compression of large additive manufacturing experimental and simulation datasets. Comput Mech 2019;63(3):491–510.
[17] Kohonen T. The self-organizing map. Proc IEEE 1990;78(9):1464–80.
[18] Kohonen T. The self-organizing map. Neurocomputing 1998;21(1–3):1–6.
[19] Rauber A, Merkl D, Dittenbach M. The growing hierarchical self-organizing map: exploratory analysis of high-dimensional data. IEEE Trans Neural Netw 2002;13(6):1331–41.
[20] Koishi M, Kowatari N, Figliuzzi B, Faessel M, Willot F, Jeulin D. Computational material design of filled rubbers using multi-objective design exploration. In: Proceedings of the 10th European Conference on Constitutive Models for Rubbers (ECCMR); 2017 Aug 28–31; Munich, German; 2017.
[21] Vesanto J, Alhoniemi E. Clustering of the self-organizing map. IEEE Trans Neural Netw 2000;11(3):586–600.
[22] Wolff SJ, Gan Z, Lin S, Bennett JL, Yan W, Hyatt G, et al. Experimentally validated predictions of thermal history and mechanical properties in laser-deposited Inconel 718 on carbon steel. Addit Manuf 2019;27:540–51.
[23] Gan Z, Liu H, Li S, He X, Yu G. Modeling of thermal behavior and mass transport in multi-layer laser additive manufacturing of Ni-based alloy on cast iron. Int J Heat Mass Transfer 2017;111:709–22.
[24] Gan Z, Yu G, He X, Li S. Surface-active element transport and its effect on liquid metal flow in laser-assisted additive manufacturing. Int Commun Heat Mass Transf 2017;86:206–14.
[25] Chew YX, Song J, Bi G, Chen HC, Yao X, Zhang B, et al. Thermal and fluid field modelling for laser aided additive manufacturing. In: Proceedings of Lasers in Manufacturing Conference 2017; Munich, German; 2017.
[26] Hunt JD, editor. Solidification and casting of metals. London: Metal Society; 1979.
[27] DebRoy T, Wei HL, Zuback JS, Mukherjee T, Elmer JW, Milewski JO, et al. Additive manufacturing of metallic components—process, structure and properties. Prog Mater Sci 2018;92:112–224.
[28] Vesanto J, Himberg J, Alhoniemi E, Parhankangas J. Self-organizing map in Matlab: the SOM toolbox. In: Proceedings of the Matlab DSP Conference; 1999 Nov 16–17. Espoo, Finland; 1999. p. 35–40.
[29] Mukherjee T, Zuback JS, De A, DebRoy T. Printability of alloys for additive manufacturing. Sci Rep 2016;6(1):19717.